



Cosmicflows-3: Two Distance–Velocity Calculators

Ehsan Kourkchi¹, H el ene M. Courtois², Romain Graziani², Yehuda Hoffman³, Daniel Pomar ede⁴, Edward J. Shaya⁵, and R. Brent Tully¹

¹Institute for Astronomy, University of Hawaii, 2680 Woodlawn Drive, Honolulu, HI 96822, USA

²University of Lyon, UCB Lyon 1, CNRS/IN2P3, IUF, IP2I Lyon F-69622, France

³Racah Institute of Physics, Hebrew University, Jerusalem, 91904 Israel

⁴Institut de Recherche sur les Lois Fondamentales de l'Univers, CEA, Universit e Paris-Saclay, F-91191 Gif-sur-Yvette, France

⁵University of Maryland, Astronomy Department, College Park, MD 20743, USA

Received 2019 August 30; revised 2019 December 9; accepted 2019 December 14; published 2020 January 23

Abstract

Tools are provided at the Extragalactic Distance Database website which provide relationships between the distances and velocities of galaxies based on smoothed versions of the velocity fields derived by the Cosmicflows program.

Unified Astronomy Thesaurus concepts: Galaxy distances (590); Observational cosmology (1146); Large-scale structure of the universe (902); Astronomy data visualization (1968)

1. Introduction

Galaxy velocities deviate from Hubble-Lema tre expansion. Deviations can be considerable, as evidenced by the motion of the Local Group of 631 km s^{-1} with respect to the rest frame of the cosmic microwave background (CMB; Fixsen et al. 1996). There are numerous instances, particularly nearby, when it is useful to have a better approximation between observed velocities and physical distances than provided by the simple assumption of uniform cosmic expansion.

The NASA/IPAC Extragalactic Database (NED) has provided estimates of galaxy distances given observed velocities based on a model by Mould et al. (2000). In alternatives, deviations are induced by up to three mass concentrations, associated with the Virgo Cluster, the Great Attractor, and the Shapley Concentration. The parameters of this model are the positions of the mass centers, the velocities induced at our location by each, and the assumption that the masses have spherically symmetric geometry with density gradients $\rho(x) \propto r^{-2}$, where r is the distance from a mass center.

This model has a direct lineage from models by Faber & Burstein (1988), Han & Mould (1990), and Han (1992). The latter of these, although it does not entertain the Shapley Concentration, considers added details, the most important being the local velocity anomaly (Faber & Burstein 1988; Tully 1988). These early studies surmised that this feature is related to the proximity of the Local Void (see also Lahav et al. 1988), a proposal that has now been robustly confirmed (Rizzi et al. 2017; Anand et al. 2019; Tully et al. 2019). Already, then, the Han (1992) model and variants capture the major features affecting the local velocity field, although another player to have emerged is the vast underdensity at the CMB dipole anti-apex, the Dipole Repeller (Hoffman et al. 2017), and the Perseus–Pisces filament (Haynes & Giovanelli 1988) significantly inhibits the flow in the CMB dipole direction.

Many other contributions could be entertained (Coma, Horologium–Reticulum, Hercules, etc.). It should be clear that any parametric model with a moderate number of parameters will only crudely approximate the peculiar velocity field. Also, for a model to be useful to the community, it should be relatively painless and efficient for a user to acquire the desired

information for a random target. The facility to be described is based on a velocity field responding to the full complexity of structure on scales of 1–200 Mpc. Two models are offered. One restricted to 38 Mpc is based on a fully nonlinear analysis. The other extending to 200 Mpc is derived from an analysis in the linear dynamical regime. Both are publicly accessible at the interactive platform to be described.

2. Distance–Velocity Users Manual

Details of the two underlying models will be discussed in the next section, but the user interface functions are the same for both. The facility can be accessed at the Extragalactic Distance Database (EDD).⁶

A user can enter the celestial coordinates of a target with a choice of coordinate systems. Examples are shown in Figures 1 and 2. Observational data from the Cosmicflows-3 compendium of distances (Tully et al. 2016) can be displayed in a cone chosen by the user centered on the target. A blue locus plots the averaged expectation velocity along the line of sight as a function of distance.⁷ Cursor control can access specific distance and velocity values along the locus. Hovering over a datum gives name, velocity, and distance specifics for that item. Zoom and translation functions are activated by side-panel toggles.

The red dashed, straight line in every plot shows the relationship between velocity and distance with uniform expansion if the Hubble Constant is $75 \text{ km s}^{-1} \text{ Mpc}^{-1}$. This line is for illustrative purposes only! Velocities and distances are determined completely independently of each other in the Cosmicflows-3 compilation. The models make no assumption about the value of H_0 .

The distance–velocity tool does not directly give peculiar velocities, V_{pec} . The tool gives expectation distances, d , at observed velocities, V_{obs} (or expectation observed velocities at specified distances). To a reasonable approximation,

⁶ <http://edd.ifa.hawaii.edu>

⁷ All distances in this tool are luminosity distances, d_L , related through redshift, z , to comoving distances, d_m , by the equation $d_L = d_m(1 + z)$.

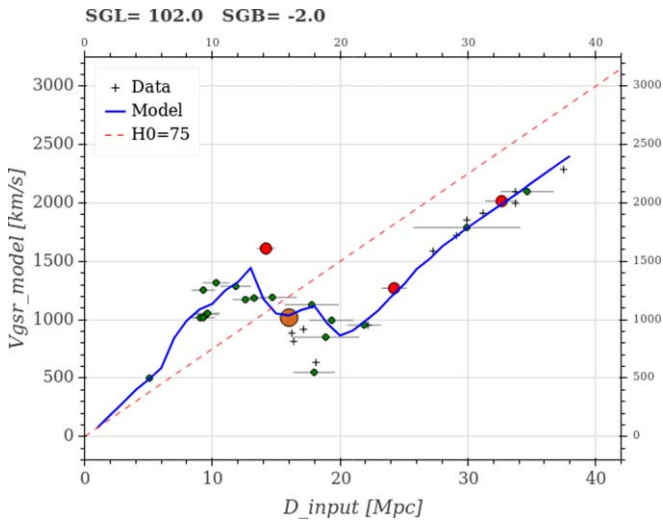


Figure 1. Velocities as a function of distance in the direction of the Virgo Cluster plotted with the nonlinear numerical action calculator. The Virgo Cluster lies at 16.0 Mpc with $V_{\text{gsr}} = 1096 \text{ km s}^{-1}$. The blue curve from the model is noisy because the number of local constraints is small at each step in the averaging but the characteristic triple-value curve (three distances sharing the same observed velocity) associated with infall around a massive cluster is clear. The red dashed line assumes $H_0 = 75 \text{ km s}^{-1} \text{ Mpc}^{-1}$. Data constraining the model are shown as large red circles if distance uncertainties are 5% or less (brown extra large circles for Virgo and Fornax clusters), and as small green circles if uncertainties are over 5% but not more than 15%. Data with larger uncertainties are represented by black plus signs but do not constrain the model.

$V_{\text{obs}} = H_0 d + V_{\text{pec}}$.⁸ It has been demonstrated (Tully et al. 2016) that Cosmicflows-3 distances and velocities are compatible with $H_0 = 75 \text{ km s}^{-1} \text{ Mpc}^{-1}$, with zero-point uncertainty at the level of 3%. Users interested in peculiar velocities can contemplate applying alternative values of H_0 at their risk. Note that altering the zero-point associated with Cosmicflows distances alters the H_0 value that would be most consistent, but the products $H_0 d$ would be unchanged. Hence, the relationship between V_{obs} and V_{pec} given in the formula above is independent of the zero-point calibration.

The reference velocities are different for the two models. In the case of the local nonlinear model, velocities are with respect to the Galactic center. With the large-scale linear model, velocities are with respect to the Local Group. Justifications for these choices will be given in the section discussing the models. In any event, it must be noted that there are variants of both these reference frames in the literature. The definition of the Galactic Standard of Rest (gsr) depends on the distance of the Galactic center and the amplitude of Galactic rotation at the Sun, as well as a small solar deviation. There are alternative choices (de Vaucouleurs et al. 1991; Eisenhauer et al. 2005; Reid et al. 2009). Our model is based on the solution by van der Marel et al. (2012). As a measure of the uncertainties inherent in the translation to the Galactic rest frame, differences between the four cited alternatives are $12 \pm 5 \text{ km s}^{-1}$.

Similarly, there are alternative versions of the Local Group rest frame (Yahil et al. 1977; Karachentsev & Makarov 1996; Courteau & van den Bergh 1999). We prefer a variant we call the Local Sheet (ls) reference frame (Tully et al. 2008). The

⁸ Davis & Scrimgeour (2014) discuss the more rigorous formulation $V_{\text{pec}} = (f(z)V_{\text{obs}} - H_0 d)/(1 + H_0 d/c)$, where $f(z)$ is given by Equation (2). Differences from the approximate formula grow with z to $\sim 30 \text{ km s}^{-1}$ by $z = 0.05$.

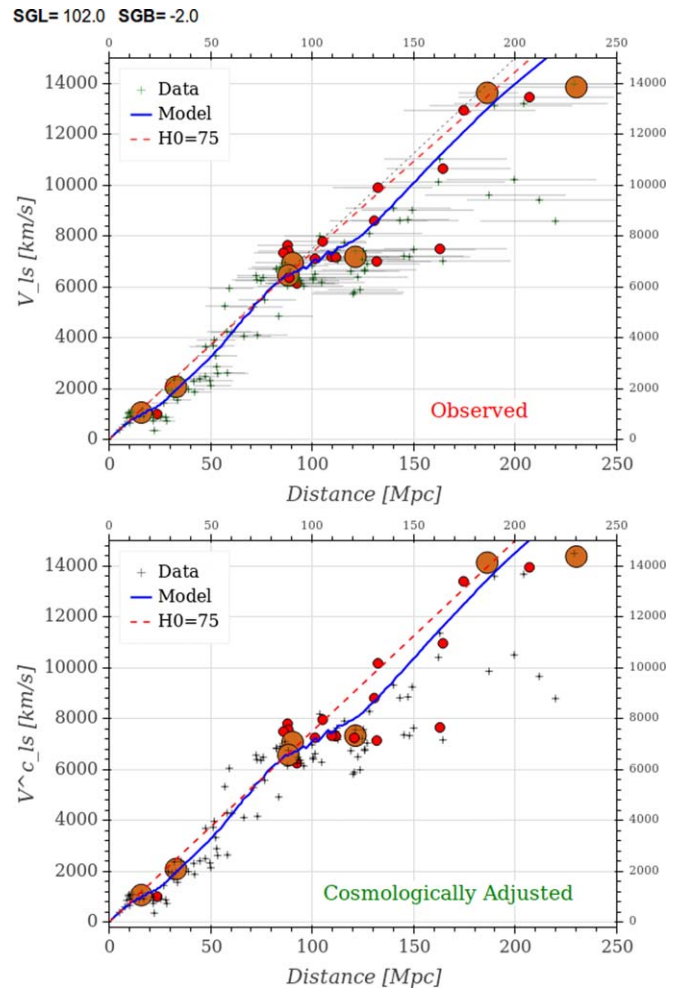


Figure 2. Velocities as a function of distance plotted with the linear calculator. Cosmological corrections become noticeable in this extended domain; the two panels give alternate representations (see the text). The blue curve is derived from interpolation of velocities on a grid of distances with intervals of 6.25 Mpc, where the value at each point is averaged over the eight nearest grid points weighted by the inverse square of separation. In the top panel, velocities are the observed values in the Local Sheet frame and the red dashed locus of constant H_0 has curvature away from the gray dotted straight line. In the bottom panel, velocities are adjusted for the cosmological effect and the red dashed Hubble line is straight. In the two panels of this figure, the data are coded by the mass of entities: large brown circles if mass is greater than $10^{14} M_{\odot}$, smaller red circles if mass is between 10^{13} and $10^{14} M_{\odot}$, and black plus signs if mass is below $10^{13} M_{\odot}$. The coordinates are chosen to be the same as in Figure 1. Major clusters in the cone in this direction are the Virgo Cluster at 16 Mpc and Abell 1367 at 88 Mpc.

three former (Local Group) solutions are derived from the properties of galaxies within 1 Mpc. The ls solution is derived from the properties of galaxies outside 1 Mpc yet within 5 Mpc. See Tully et al. (2008) for the argument that this solution is the most stable. Uncertainties between the alternative Local Group frames are at the level of $19 \pm 10 \text{ km s}^{-1}$.

The linear model extends to velocities of 15,000 km s^{-1} and cosmological corrections reach $\sim 4\%$. The corrected velocity V_{ls}^c is related to the observed velocity V_{ls} by

$$V_{\text{ls}}^c = f(z) V_{\text{ls}}, \quad (1)$$

where

$$f(z) = 1 + 1/2(1 - q_0)z - 1/6(2 - q_0 - 3q_0^2)z^2 \quad (2)$$

$$q_0 = 1/2(\Omega_m - 2\Omega_\Lambda) = -0.595 \quad (3)$$

when $\Omega_m = 0.27$ and $\Omega_\Lambda = 0.73$ and $z = V_{ls}/c$ (Wright 2006).

In the top panel of Figure 2 velocities are observed values (averaged over group members) but in this representation there is a slight curvature of the Hubble relation manifested in the departure of the red dashed curve from the faint gray straight line. Velocities in the bottom panel are increased by the cosmological correction so the red dashed Hubble line is straightened. In detail the correction depends on the choices of the cosmological matter and energy density parameters Ω_m and Ω_Λ , but differences in the correction between reasonable values of these parameters are negligible within the velocity range being considered. $f(z = 0.05)$ decreases by 0.1% if Ω_m increases and Ω_Λ decreases by 0.03.

Hover with the cursor over a datum element of the linear model to obtain input distance and velocity information. The element may be an individual galaxy or a group and is identified by the parameter PGC1, the Principal Galaxies Catalog identification (de Vaucouleurs et al. 1991) of the brightest member. The Nest parameter identifies the membership of elements in the Two Micron All Sky Survey (2MASS) group catalog of Tully (2015a).

For convenience, formulae are given here for conversions between heliocentric velocities, V_h , and the reference frames used in the distance–velocity tools where the angles are Galactic longitude and latitude (l, b).

gsr:

$$V_{gsr} = V_h + 11.1 \cos l \cos b + 251 \sin l \cos b + 7.25 \sin b \quad (4)$$

ls:

$$V_{ls} = V_h - 26 \cos l \cos b + 317 \sin l \cos b - 8 \sin b. \quad (5)$$

Between gsr and ls:

$$V_{ls} = V_{gsr} - 37 \cos l \cos b + 66 \sin l \cos b - 15 \sin b. \quad (6)$$

3. Models

Two calculators are offered: one limited to distances less than 38 Mpc ($V_{obs} \sim 2850 \text{ km s}^{-1}$) based on a fully nonlinear dynamical model and the other extending to 200 Mpc ($15,000 \text{ km s}^{-1}$) at lower resolution and based on a linear model.

3.1. Nonlinear Model Limited to 38 Mpc

This calculator presents a smoothed version of the current day ($z = 0$) velocity field derived from the numerical action orbit reconstruction of Shaya et al. (2017). In brief summary, orbits are followed for 1382 tracers (either groups or individual galaxies) that collectively dominate the mass content associated with luminosity within 38 Mpc $\simeq 2850 \text{ km s}^{-1}$. The tracers are either (or both) important mass constituents or have very accurately known distances (15% or better uncertainties in the Cosmicflow-3 compendium). Physically consistent orbits are followed from $z = 4$ to $z = 0$. The orbit reconstruction is embedded in a tidal field at distances greater than 38 Mpc based on the Cosmicflows-2 velocity model of Tully et al. (2014).

There can be no hope of untangling the complexity of orbits after shell crossing, so orbits describe the centers of mass of the ensemble of a group today. The initial distribution at $z = 4$ of our sample is well dispersed, but by today the entities have become concentrated in the current observed structure. For practical reasons, the density of tracers is highest nearby. Consequently, the model is most robust within ~ 15 Mpc and is poorly sampled in the voids.

The orbits of our Galaxy and Andromeda (M31) are followed separately in the numerical action model of Shaya et al. (2017). These galaxies are each the central host of distinct collapsed halos. We (Tully 2015b; Kourkchi & Tully 2017) equate groups with collapsed halos; the term ‘‘Local Group’’ is a misnomer. The gsr is the natural coordinate system for studies of the orbital history of the Milky Way.

The model distance–velocity curve (blue) is derived from interpolation of the model velocities on a grid of distances with grid intervals of 0.2 Mpc at the origin increasing to 1 Mpc intervals at 38 Mpc, the outer limit of the model. The value at a grid point is averaged over the four nearest mass points weighted by the inverse square of separation. Pause the cursor over the blue curve for distance and velocity information at a chosen location. Pause the cursor over individual entries for information on data points.

3.2. Linear Model Extending to 200 Mpc

This second calculator is based on the three-dimensional velocity and density fields of Graziani et al. (2019). The likelihood model seeks consistency between velocities and the matter distribution in the linear regime of a direct relationship between the gradient of the velocity field and densities. The procedure is an extension of that by Lavaux (2016). Care is taken to negate Malmquist bias (Strauss & Willick 1995) and the asymmetry in velocity errors in translations to distance from the logarithmic modulus. Multiple constrained realizations are averaged following Hoffman & Ribak (1991).

Cosmicflows-3 provides distance and velocity measures. The 17,647 individual galaxy entries are collected into 11,501 entities through grouping, with two or more galaxies with distance estimates in 1704 groupings.⁹ Linkages are established between galaxies with distance estimates and a 2MASS group catalog (Tully 2015a). A group is assigned the weighted average distance of the available measures and the averaged velocity of all known members. As a consequence, although distances to individual galaxies can have large uncertainties, there are a multitude of groups that are relatively well constrained. The dynamically dominant groups with distance measures are identified by larger symbols in the displays of the linear model in plots analogous to Figure 2.¹⁰

The present Graziani et al. (2019) model is constructed on a relatively coarse grid at 6.25 Mpc spacings. There remains an issue of limited observations at latitudes within 15° of the plane of our Galaxy. Nearby, within $\sim 8000 \text{ km s}^{-1}$, our filtered reconstruction is relatively successful across this zone. However, at greater distances the gap of the zone of obscuration becomes too large for a good reconstruction.

⁹ The exact numbers of individual and grouped entities change as minor corrections are made. See <http://edd.ifa.hawaii.edu> for updated catalogs.

¹⁰ Beyond $10,000 \text{ km s}^{-1} \sim 130$ Mpc the group mass assignments from Tully (2015a) become unreliable because correction factors for missing components become very large.

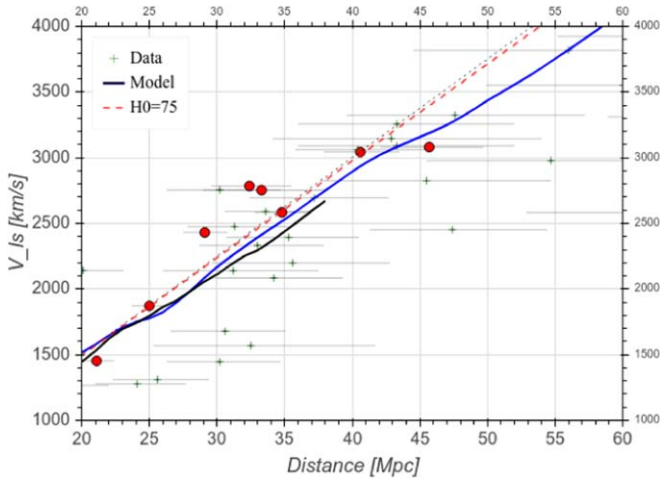


Figure 3. Zoomed extraction from the distance–velocity calculator in the direction of the galaxy NGC 4993. The result from the nonlinear calculator terminating at 38 Mpc is overlaid as a black curve on the result from the linear calculator. Departures from the Hubble expectation with the linear model are $\sim -100 \text{ km s}^{-1}$ nearward of $\sim 42 \text{ Mpc}$, increasing in amplitude to $\sim -300 \text{ km s}^{-1}$ longward of that point.

The ls (or alternative Local Group) reference frame is preferred in this model because of the cancellation of the Milky Way and M31 motions toward each other. Averaged velocities are appropriate in the linear regime. Nearby galaxies have modest dispersions in the ls frame (Karachentsev et al. 2002). All nearby galaxies share similar large peculiar motions in the frame of the CMB.

4. Practical Example

As an example of the service that the distance–velocity calculator provides, consider an effort to determine the Hubble Constant from a measurement of the distance to the gravitational wave event GW170817 that occurred in the galaxy NGC 4993 (Abbott et al. 2017). By happenstance, the distance, $d \sim 40 \text{ Mpc}$, is at the extremity of coverage provided by the nonlinear model (although that model is embedded within the 100 Mpc scale tidal field deduced from a linear analysis of Cosmicflows-2). It comfortably lies within the domain of coverage of the new linear model.

What is the appropriate velocity to accompany the distance measurement for an estimate of the Hubble Constant? It is important to understand the environment of the target on a range of scales. Most immediately, does the target lie in a group? In the case of NGC 4993, yes, this galaxy lies in a group with the dominant member NGC 4970. The group is identified as HDC 751 (Crook et al. 2007), 2M++ 1294 (Lavaux & Hudson 2011), Nest 100214 (Tully 2015a), and PGC1 45466 (Kourkchi & Tully 2017). In the latter catalog, there are 22 galaxies linked with the group, with $\langle V_{\text{helio}} \rangle = 2995 \pm 25 \text{ km s}^{-1}$. In alternate reference frames of interest, $\langle V_{\text{gsr}} \rangle = 2851 \text{ km s}^{-1}$, $\langle V_{\text{ls}} \rangle = 2783 \text{ km s}^{-1}$, and $\langle V_{\text{cmb}} \rangle = 3308 \text{ km s}^{-1}$.

On a larger scale, this PGC1 45466 = NGC 4970 group lies roughly along the line of sight toward the Great Attractor (Dressler et al. 1987), 18° ($\sim 13 \text{ Mpc}$) removed from the dominant Centaurus Cluster ($d = 40.5 \pm 1.6 \text{ Mpc}$, $V_{\text{ls}} = 3285 \text{ km s}^{-1}$). There is a clear infall pattern in the line of sight toward the Centaurus Cluster, with objects to the immediate foreground falling away from us toward the cluster

and objects behind manifesting backside infall toward us. This effect extends in a weakened fashion to the NGC 4993 line of sight. At a distance of around 40 Mpc, there is ambiguity whether the NGC 4970 group with NGC 4993 is frontside falling away or backside falling forward with respect to the overdensity around the Centaurus Cluster. Figure 3 is extracted from the distance–velocity calculator in the NGC 4993 direction, with the nonlinear solution superimposed on the linear solution. There is close agreement between the two at distances less than 30 Mpc. At greater distances the nonlinear model runs about 100 km s^{-1} below the linear model but the nonlinear model is poorly constrained at its edge of application. Considering the linear model, within 10 Mpc foreground of $\sim 40 \text{ Mpc}$ observed velocities are running about 100 km s^{-1} below the $H_0 = 75$ fiducial line while by 50 Mpc the observed velocities drop to about 300 km s^{-1} below the fiducial line. The consequence is an ambiguity due to this Centaurus Cluster overdensity infall pattern. The amplitude of the wave is 200 km s^{-1} in the linear regime (and greater if nonlinear effects would be taken into account).

It is most common to derive estimates of the Hubble Constant in the reference frame of the CMB. However nearby galaxies are participating in a coherent flow, a coherence that extends to include the NGC 4970 group with NGC 4993 as a member. A correction for the flow is required if working in the CMB frame that is closely equivalent to working without a correction in the ls (Local Group) frame. This comment is a cautionary reminder of the jeopardy of evaluating the Hubble Constant locally. Should we live in a large scale under- or over density, it would be necessary to make measurements beyond this feature to be comfortable in the CMB frame.

Finally, it is to be appreciated that the distances in this distance–velocity calculator are based on a specific zero-point calibration that may or may not pass the test of time. The $H_0 = 75 \text{ km s}^{-1} \text{ Mpc}^{-1}$ fiducial line is consistent with the current Cosmicflows-3 data compilation. A user of the distance–velocity calculator may have a distance that is implicitly based on a different zero-point scale. However, as discussed in Section 2, peculiar velocities are decoupled from the Hubble Constant. A user can consider the distance–velocity calculator distance scale to be elastic, with the fiducial Hubble line flexing accordingly, but the peculiar velocity amplitudes with respect to the fiducial line will be unchanged at a given observed velocity.

In review of the case for NGC 4993, as a best effort at accounting for deviations from cosmic expansion, an estimate can be made of the value of the Hubble Constant, $H_0 = (V_{\text{obs}} - V_{\text{pec}})/d$ taking $V_{\text{obs}} = 2783 \text{ km s}^{-1}$, the value for the NGC 4970 group, and V_{pec} somewhere between -100 and -300 depending on the user’s preferred distance and whether that places the target foreground or background to the Centaurus Cluster overdensity.

5. Future Augmentations

Cosmicflows is a continuously evolving program. It is anticipated that the distance–velocity calculators will be updated at intervals. The resolution can be improved with greater computational effort. In combination, the quasi-linear methodology of Hoffman et al. (2018) can be exploited. There is the intention of extending the numerical action orbit reconstruction model of Shaya et al. (2017) to 100 Mpc.

Cosmicflows-4 is on the horizon, with constraints to be provided by $\sim 30,000$ distances.

The latest models will be made available at the EDD.¹¹

Many people have contributed directly or indirectly to this substantial undertaking. Special thanks to Gagandeep Anand, Igor Karachentsev, Dmitry Makarov, Lidia Makarova, Don Neill, Luca Rizzi, Mark Seibert, Kartik Sheth, and Po-Feng Wu. This catalog could hardly have been assembled without the resources of NED, the NASA/IPAC Extragalactic Database, and the Lyon extragalactic database HyperLeda. Financial support for the Cosmicflows program has been provided by the US National Science Foundation award AST09-08846, an award from the Jet Propulsion Lab for observations with *Spitzer Space Telescope*, and NASA award NNX12AE70G for analysis of data from the *Wide-field Infrared Survey Explorer*. Additional support has been provided by the Lyon Institute of Origins under grant ANR-10-LABX-66 and the CNRS under PICS-06233 and the Israel Science Foundation grant ISF 1358/18.

ORCID iDs

Ehsan Kourkchi  <https://orcid.org/0000-0002-5514-3354>
 H el ene M. Courtois  <https://orcid.org/0000-0003-0509-1776>
 Daniel Pomar ede  <https://orcid.org/0000-0003-2038-0488>
 Edward J. Shaya  <https://orcid.org/0000-0002-3234-8699>
 R. Brent Tully  <https://orcid.org/0000-0002-9291-1981>

References

Abbott, B. P., Abbott, R., Abbott, T. D., et al. 2017, *Natur*, **551**, 85
 Anand, G. S., Tully, R. B., Rizzi, L., Shaya, E. J., & Karachentsev, I. D. 2019, *ApJ*, **880**, 52
 Courteau, S., & van den Bergh, S. 1999, *AJ*, **118**, 337
 Crook, A. C., Huchra, J. P., Martimbeau, N., et al. 2007, *ApJ*, **655**, 790

Davis, T. M., & Scrimgeour, M. I. 2014, *MNRAS*, **442**, 1117
 de Vaucouleurs, G., de Vaucouleurs, A., Corwin, H. G., Jr., et al. 1991, Third Reference Catalogue of Bright Galaxies, Vol. 1–3 (Berlin Heidelberg New York: Springer-Verlag)
 Dressler, A., Faber, S. M., Burstein, D., et al. 1987, *ApJL*, **313**, L37
 Eisenhauer, F., Genzel, R., Alexander, T., et al. 2005, *ApJ*, **628**, 246
 Faber, S. M., & Burstein, D. 1988, in *Large-scale Motions in the Universe*, ed. V. C. Rubin & G. V. Coyne (Princeton, NJ: Princeton Univ. Press), **115**
 Fixsen, D. J., Cheng, E. S., Gales, J. M., et al. 1996, *ApJ*, **473**, 576
 Graziani, R., Courtois, H. M., Lavaux, G., et al. 2019, *MNRAS*, **488**, 5438
 Han, M. 1992, *ApJ*, **395**, 75
 Han, M., & Mould, J. 1990, *ApJ*, **360**, 448
 Haynes, M. P., & Giovanelli, R. 1988, in *Large-scale Motions in the Universe*, ed. V. C. Rubin & G. V. Coyne (Princeton, NJ: Princeton Univ. Press), **31**
 Hoffman, Y., Carlesi, E., Pomar ede, D., et al. 2018, *NatAs*, **2**, 680
 Hoffman, Y., Pomar ede, D., Tully, R. B., & Courtois, H. M. 2017, *NatAs*, **1**, 0036
 Hoffman, Y., & Ribak, E. 1991, *ApJL*, **380**, L5
 Karachentsev, I. D., & Makarov, D. A. 1996, *AJ*, **111**, 794
 Karachentsev, I. D., Sharina, M. E., Makarov, D. I., et al. 2002, *A&A*, **389**, 812
 Kourkchi, E., & Tully, R. B. 2017, *ApJ*, **843**, 16
 Lahav, O., Lynden-Bell, D., & Rowan-Robinson, M. 1988, *MNRAS*, **234**, 677
 Lavaux, G. 2016, *MNRAS*, **457**, 172
 Lavaux, G., & Hudson, M. J. 2011, *MNRAS*, **416**, 2840
 Mould, J. R., Huchra, J. P., Freedman, W. L., et al. 2000, *ApJ*, **529**, 786
 Reid, M. J., Menten, K. M., Zheng, X. W., et al. 2009, *ApJ*, **700**, 137
 Rizzi, L., Tully, R. B., Shaya, E. J., Kourkchi, E., & Karachentsev, I. D. 2017, *ApJ*, **835**, 78
 Shaya, E. J., Tully, R. B., Hoffman, Y., & Pomar ede, D. 2017, *ApJ*, **850**, 207
 Strauss, M. A., & Willick, J. A. 1995, *PhR*, **261**, 271
 Tully, R. B. 1988, *Natur*, **334**, 209
 Tully, R. B. 2015a, *AJ*, **149**, 171
 Tully, R. B. 2015b, *AJ*, **149**, 54
 Tully, R. B., Courtois, H., Hoffman, Y., & Pomar ede, D. 2014, *Natur*, **513**, 71
 Tully, R. B., Courtois, H. M., & Sorce, J. G. 2016, *AJ*, **152**, 50
 Tully, R. B., Pomar ede, D., Graziani, R., et al. 2019, *ApJ*, **880**, 24
 Tully, R. B., Shaya, E. J., Karachentsev, I. D., et al. 2008, *ApJ*, **676**, 184
 van der Marel, R. P., Fardal, M., Besla, G., et al. 2012, *ApJ*, **753**, 8
 Wright, E. L. 2006, *PASP*, **118**, 1711
 Yahil, A., Tammann, G. A., & Sandage, A. 1977, *ApJ*, **217**, 903

¹¹ <http://edd.ifa.hawaii.edu>